Scientia Horticulturae 322 (2023) 112398

Contents lists available at ScienceDirect

Scientia Horticulturae

journal homepage: www.elsevier.com/locate/scihorti

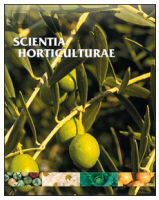

The role of LAI and leaf chlorophyll on NDVI estimated by UAV in grapevine canopies

Giovanni Caruso, Giacomo Palai *, Letizia Tozzini, Claudio D'Onofrio, Riccardo Gucci

Department of Agriculture Food and Environment, University of Pisa, Via del Borghetto, 80, 56124, Pisa, Italy

ARTICLE INFO

Keywords:
Unmanned aerial vehicle
Canopy volume
Leaf area index
Normalized Difference Vegetation Index
Projected canopy area
Vitis vinifera L.

ABSTRACT

Despite the wide use of the Normalized Difference Vegetation Index (NDVI) in precision viticulture, there are no studies aimed at discriminating the contribution of plant biomass from that of leaf chlorophyll on canopy NDVI. Leaf area index (LAI) and leaf chlorophyll (Chl) were concomitantly monitored by ground measurements and projected canopy area (PCA), canopy volume (CV) and NDVI by high resolution UAV multispectral images in fully productive "Sangiovese" grapevines either grown in containers or in the field and subjected to different irrigation regimes over two consecutive years. NDVI values calculated from only vine canopy pixels ($NDVI_{UAV}$) and NDVI obtained from mixed ground-canopy pixels (simulated Satellite NDVI, $NDVI_{SAT}$) were both evaluated as potential predictor of LAI and leaf Chl concentration.

The seasonal patterns of LAI and leaf Chl concentration were affected by irrigation, showing differences depending on field vs container-grown conditions. In situations where a decoupling between LAI and leaf Chl occurred, $NDVI_{UAV}$ and $NDVI_{SAT}$ showed different responses: $NDVI_{UAV}$ patterns strictly followed the leaf Chl ones, whereas $NDVI_{SAT}$ was more affected by LAI. The coefficient of determination between $NDVI_{UAV}$ and leaf Chl ranged between 0.51 and 0.78, that between $NDVI_{UAV}$ and leaf Chl from 0.01 to 0.76, depending on the irrigation-growing conditions combination. $NDVI_{SAT}$ was a better predictor of LAI (R^2=0.69) than $NDVI_{UAV}$ (R^2=0.42). In field-grown vines the relationships between NDVI (both UAV and SAT) and LAI was stronger than in potted ones. The relationships between LAI and PCA (R^2=0.44) or LAI and canopy volume (R^2=0.77) were both significant. The results allowed to confirm the two main hypotheses behind this experiment: i) leaf Chl concentration had a greater impact than LAI on NDVI values obtained from vine canopy pixels ($NDVI_{UAV}$), whereas $NDVI_{SAT}$ was more affected by LAI; ii) The canopy volume from UAV images was a better predictor of LAI than NDVI and the resulting relationship showed a better temporal stability.

1. Introduction

Remote sensing is increasingly used as a non-invasive method for estimating physiological and biophysical plant parameters based on the spectral canopy signatures which tend to vary under different environmental conditions and cultural practices (Haboudane et al., 2004; Zarco-Tejada et al., 2005). In this respect, vegetative indices (VIs) have been developed as the combination of various spectral bands and they are widely used due to their easy derivation and applicability. Among the VIs, the Normalized Difference Vegetation Index (NDVI) is still the most widely used indicator of vegetative vigor in remote sensing (Bramley, 2001; Elazab et al., 2016; Caruso et al., 2019; Tan et al., 2020; Matese and Di Gennaro, 2021). NDVI is based on different radiation absorption by green biomass in red and near-infrared (NIR) wavebands according to the formula proposed by Rouse et al. (1974).

Chlorophyll (Chl) has strong absorbance peaks in the red and blue regions of the spectrum. The blue peak overlaps with the absorbance of the carotenoids and, thus, it is generally not used for estimation of chlorophyll content. The intercellular arrangement of the leaf mesophyll and canopy structure are the most important factors determining canopy NIR reflectance (Sims and Gamon, 2002; Gitelson et al., 2004). Healthy leaves absorb most of the incident visible radiation, particularly in the red region and reflect and transmit most incident NIR light. Hence, NDVI has been widely used for estimating leaf chlorophyll and photosynthetically active vegetation coverage.

NDVI can be calculated from aerial images acquired from different aerial platforms, such as unmanned vehicles (UAVs), airborne or satellites (Johnson et al., 2003; Matese et al., 2015; Campos et al., 2021).

* Corresponding author.
E-mail address: giacomo.palai@phd.unipi.it (G. Palai).

https://doi.org/10.1016/j.scienta.2023.112398
Received 27 March 2023; Received in revised form 28 July 2023; Accepted 4 August 2023
Available online 12 August 2023

UAV platforms are characterized by the high flexibility in flight scheduling, low operational costs and high spatial ground resolution of the acquired images. On the other hand, their limited payload and short flight time represent the main constraints for their application to medium or large-sized farms. Satellite surveys allow to map large areas with a single image which, however, has a low spatial resolution and can suffer from cloud cover. Differences in geometrical image resolution also affect NDVI values as it can be derived from vine canopy pixels (UAV) or from mixed ground-canopy pixels (satellite). In the first case, the NDVI refers to canopies only, whereas the NDVI derived from satellite images represents an average NDVI value of canopy and ground within each pixel (Di Gennaro et al., 2019; Khaliq et al., 2019)

Previous studies in fruit orchards and vineyards tested the ability of remotely sensed NDVI in estimating grapevine leaf area (Johnson et al., 2003; Rey-Caramès et al., 2015; Caruso et al., 2017, 2019; White et al., 2019), pruning weight (Dobrowski et al., 2003; Bonilla et al., 2015), leaf biochemical compounds concentration (Zarco-Tejada et al., 2005; Caruso et al., 2017), yield and fruit quality (Lamb et al., 2004; Sun et al., 2017; Caruso et al., 2021; Matese and Di Gennaro 2021, 2022a). Rey--Caramès et al. (2015) tested the capability of UAV multispectral imagery to assess the vegetative spatial variability within a vineyard and measured a Pearson's correlation coefficient of 0.49 when NDVI was plotted against grapevine leaf area. Better correlations for the same relationship were obtained using satellite images by Johnson et al. (2003).

As for the leaf Chl concentration, Caruso et al. (2017) reported a significant correlation between NDVI estimated from UAV images and leaf chlorophyll of field-grown Sangiovese grapevines measured at fruit-set completed and at the beginning of bunch closure, over a wide range of chlorophyll concentrations (from 0.30 to 0.53 g dm^{-2}). In the same study no significant NDVI-leaf chlorophyll correlation was observed after veraison when leaf chlorophyll values ranged from 0.42 to 0.50 g dm^{-2}. In a recent three-year experiment Matese and Di Gennaro (2021) showed that the model based on geometric data derived by UAV performed better than that based on NDVI data in estimating yield, total soluble solids, and pruning weight in Sangiovese vines.

Despite the wide use of NDVI in precision viticulture there are no studies aimed at discriminating the specific impact of leaf area and leaf chlorophyll concentration on the resulting grapevine canopy NDVI. This information might be crucial when water or nutrient availability become scarce leading to a decoupling between the leaf nitrogen status and canopy biomass. In fact, despite plant nitrogen content and canopy biomass are usually correlated, a different relationship may occur under those conditions that induce an excessive leaf area (i.e. absence of water limitations). Previous studies reported cases of low plant nitrogen content in field grown vines with an excessive leaf area, indicating a possible nitrogen "dilution" within the volume of the biomass (Spring et al., 2012; Verdenal et al., 2021).

In this study LAI and leaf chlorophyll patterns were measured in grapevine under different growing conditions in order to evaluate the different impact of grapevine leaf area and leaf chlorophyll on the canopy NDVI values. It has also been tested the ability of the NDVI from mixed canopy and non-canopy pixels (simulated satellite NDVI, $NDVI_{SAT}$) and of geometrical indices derived from UAV images (projected canopy area and canopy volume) to estimate LAI in fully-productive "Sangiovese" grapevines growing outdoor under different growing conditions (potted and field grown) and subjected to different irrigation regimes. The two hypotheses behind this work were: i) canopy NDVI calculated from vine canopy pixels ($NDVI_{UAV}$) under specific conditions (high water availability and low leaf chlorophyll concentration) is more affected by the leaf chlorophyll concentration than LAI, thus losing its ability as canopy biomass predictor; ii) canopy volume from UAV images is a better predictor of LAI than $NDVI_{UAV}$ and $NDVI_{SAT}$, also in terms of temporal stability.

2. Materials and methods

2.1. Site and plant material

Two experiments were carried out over two consecutive growing seasons (2019–2020) on fully-productive grapevines (*Vitis vinifera* L.) of cultivar Sangiovese at two experimental sites characterized by different conditions: the Experiment 1 was carried out at the Colignola experimental farm of the Department of Agriculture Food and Environment of the University of Pisa (43.73° N 10.47° E, 5 m a.s.l.) using fully-productive potted grapevines; the Experiment 2 was carried out at the Bulichella farm located in Suvereto, Italy (43.07° N 10.70° E, 51 m a.s.l.) using field-grown grapevines.

In Experiment 1 seven-year old Sangiovese grapevines grafted on 110R (*V. berlandieri x V. rupestris*) were grown in 50 L containers under field conditions. Vines were spaced at 0.9 × 4.2 m distance to allow high light interception. Vines were pruned in February to retain one spur with two count buds and one cane with six to eight count buds according to the Guyot training system. Growing shoots were positioned vertically using a trellis system made of seven horizontal galvanized steel wires running along each row of containers at three different heights. Potted grapevines used for the experiments were fully comparable in terms of yield (1.8–3.2 kg $vine^{-1}$) and canopy volume (see results) to the field-grown vines used in Experiment 2 (Fig. 1). Climatic conditions were monitored using a WatchDog (Spectrum Technologies Inc, Aurora IL, USA) weather station installed on site (Supplemental Table 1). Starting from two weeks before bud burst, vine phenology was monitored every four or five days to determine the dates of bud burst (DOY 95 and 93 in 2019 and 2020), fruit set (62 and 55 days after bud burst, DABB, in 2019 and 2020, respectively) and veraison (occurred between 116 and 129 DABB in 2019 and between 115 and 129 DABB in 2020) according to Coombe et al. (1995). Differences in the veraison date were induced by irrigation treatments, as reported below. Each vine was fertilized via fertigation three times (twice before berry pea size and once 1 week after harvest) as reported by Palai et al. (2022).

Experiment 2 was performed in a 0.5 hectare commercial vineyard (cv. Sangiovese) grafted on 420A (*V. berlandieri* x *V. riparia*), planted in 2000 at 0.9 × 2.4 m spacing in a sandy-clay-loam soil. Vines were pruned in February and trained according to the Guyot system (see Experiment 1). Climatic conditions were monitored using an iMETOS IMT 300 (Pessl Instruments GmbH, Weiz, Austria) weather station installed on site (Supplemental Table 1). Vine phenology was monitored on 18 vines as previously explained to determine the dates of bud burst (DOY 91 and 88 in 2019 and 2020), fruit set (62 and 65 days after bud burst, DABB, in 2019 and 2020, respectively) and veraison (between 114 and 118 in 2019 and between 109 and 114 DABB in 2020). The vineyard was fertilized by applying composted sheep manure followed by the sowing of a cover crop (*Vicia faba* L.) after harvest.

2.2. Irrigation

In Experiment 1 all vines were fully irrigated until 63 and 66 DABB (in 2019 and 2020, respectively) when three irrigation regimes (Full Irrigation, FI; Regulated Deficit Irrigation Before Veraison, RDI-BV; Regulated Deficit Irrigation After Veraison, RDI-AF) were imposed. FI vines were fully irrigated from budburst through harvest based on actual water consumption of FI vines, measured as daily weight loss. Four representative vines were placed on four square weighing platforms with load cells and their weight loss measured at 15 min intervals. More details are reported in Caruso et al. (2022b). RDI-BV and RDI-AV vines were subjected to water deficit from fruit set through the beginning of veraison (FS-V, 30–31% of FI) and from veraison through harvest (V-H, 31–38% of FI), respectively. During the full irrigation period, all treatments were irrigated to maintain the stem water potential above −0.6 MPa. Each container received water from two emitters (2 L h^{-1} each) and vines were irrigated twice a day. More details are reported in Palai

Fig. 1. Overview of the vineyards used in the Experiment 1 and Experiment 2. Details are reported in paragraphs 2.1 and 2.2.

et al. (2022).

In Experiment 2 grapevines were fully irrigated until 66 and 69 DABB (in 2019 and 2020, respectively) when three irrigation treatments (Full Irrigation, FI; Sustained Deficit Irrigation, SDI; Rainfed, RF) were established. FI vines were fully irrigated (100% of crop evapotranspiration, ET_c) from budburst till harvest. Reference evapotranspiration (ET_0) was recorded by a meteorological station located on-site and ET_c calculated according to the formula: $ET_c = ET_0$ x Kc. The crop coefficient (Kc) assumed values of 0.25 in May and June and 0.65 from July to September. The SDI vines received about 40–45% of the irrigation volume of FI from budburst to harvest. The RF vines were not irrigated. Each vine received water from two emitters (1.6 L h^{-1} each) and were irrigated once a day.

2.3. Leaf chlorophyll concentration and grapevine leaf area

Leaf chlorophyll concentration was estimated using a Minolta Soil-Plant Analyses Development - SPAD 502 portable greenness meter (Konica Minolta Inc., Osaka, Japan) on three fully-expanded leaves (basal, median and apical) from each vine (three vines per irrigation treatment). SPAD measurements were converted to leaf Chl concentration values using the regression equation previously developed for "Sangiovese" vines (Caruso et al., 2017). In Experiment 1, leaf Chl was estimated on 9 vines at 68, 87, 99, 118, 135 and 151 DABB in 2019 and 66, 94, 104, 111, 122 and 140 DABB in 2020. In Experiment 2 on 18 vines at 69, 89, 111, 143 and 159 DABB in 2019 and 66, 92, 104, 120, 133 and 140 DABB in 2020.

The LAI was estimated using a non-destructive canopy analysis system (SunScan SS1-R3-BF3, Delta-T Devices, Cambridge, UK) following the standard protocol recommended by the manufacturer. In Experiment 1, LAI measurements were taken on 9 vines at 68, 87, 99, 118, 135 and 151 DABB in 2019 and at 66, 94, 104, 11, 122 and 140 DABB in 2020. In Experiment 2, LAI was measured on 18 vines 5 times a year (69, 89, 111, 143 and 159 DABB in 2019 and 66, 84, 104, 120 and 140 DABB). The method of estimating LAI (gap fraction inversion) is based on photosynthetically active radiation (PAR) measurements beneath the canopy using a line quantum sensor array. Each measurement consisted of equally spaced readings (0.20 m apart) at ground level, starting from the point below the canopy to the inter row (in the middle between the two adjacent rows), with the linear probe positioned parallel to the rows. LAI values obtained using this non-destructive method were checked against direct leaf area (LA) measurement of three additional representative grapevines in Experiment 1. These grapevines were subjected to progressing levels of leaf removal until the complete defoliation in order to obtain a wide range of values of LA per vine. At each level of defoliation, the number of leaf layers was determined using the Point Quadrat Analysis method (Smart and Robinson, 1991) modified to perform 100 measurements per vine using a 0.1 × 0.1 m grid, whereas the leaf area per vine was measured using the image analysis software Image J (National Institutes of Health, Bethesda, MD, USA).

2.4. Multispectral imagery acquisitions from the unmanned aerial platform

The acquisition campaign was performed using a S1000 UAV octocopter (DJI, Shenzhen, China) capable to fly autonomously over a predetermined waypoint course. The S1000 was equipped with a 2-axis stabilized gimbal carrying a multispectral camera (RedEdge MX, MicaSense Inc, Seattle, WA, USA). Images were recorded over five wavelengths intervals: Blue (455–495 nm), Green (540–580 nm), Red (658–678 nm), Red-Edge (707–727 nm), and Near Infrared (800–880 nm).

Images were acquired at 68, 87, 99, 118, 135 and 151 DABB (Experiment 1 in 2019), at 66, 80, 94, 104, 111, 122, 140 and 154 (Experiment 1 in 2020), at 69, 89, 111, 129, 143 and 159 DABB (Experiment 2 in 2019) and at 66, 84, 92, 104, 120, 133, 140 and 161 DABB (Experiment 2 in 2020).

The flight altitude was 50 m above ground level flying at 2.5 m s^{-1} speed. The ground sample distance was 34 mm $pixel^{-1}$. The image forward and side overlap (80% and 70%, respectively), guaranteed an optimal photogrammetric processing. Before the UAV flights, a set of 7 (Experiment 1) and 8 (Experiment 2) ground control points (GCPs) were placed in the vineyard and georeferenced using a Topcon Hyper HR GPS (Topcon Positioning Systems Inc., Livermore, CA, USA) able to achieve a resolution of 0.02 m.

2.5. Image processing

The three-dimensional canopy volume, the projected canopy area (PCA) and the NDVI of each vine were calculated following the same procedure reported in Caruso et al. (2017, 2019). Images were radiometrically calibrated using the images of the MicaSense calibration panel acquired on field at each date of flight and following the procedure provided by the manufacturer.

The multispectral images were processed using Agisoft Metashape Professional Edition (Agisoft LLC, St. Petersburg, Russia) for the generation of the multispectral orthophoto and the digital surface model (DSM) of the vineyard, as reported in Caruso et al. (2017).

The digital surface model (DSM) was obtained from the 3D point cloud and then processed in ArcGIS (ESRI, Redlands, CA, USA) to obtain a digital terrain model (DTM). The normalized DSM, obtained by subtracting the DTM from the DSM, allowed to retrieve the height of each three-dimensional axes of the canopy point above the ground. The vine canopy volume was calculated by subtracting the volume comprised between the ground level and 0.9 m (height of the fruiting wire) as reported in (Caruso et al., 2017). The same height was used in both potted and field grown vines. The very high-resolution images acquired allowed to separate grapevine crowns from the background. The PCA

was obtained using a height value threshold (0.9 m) which allow to distinguish soil and grapevine components. The normalized DSM was also used to extract vine canopy pixels to be used for the calculation of the Normalized Difference Vegetation Index (NDVI, Rouse et al. 1973) using ArcGIS software (ESRI, Redlands, CA, USA). NDVI was calculated using the following equation:

$$NDVI = (NIR - RED)/(NIR + RED) \quad (1)$$

2.6. Comparison between $NDVI_{uav}$ and $NDVI_{sat}$

In Experiment 1 the NDVI values of single grapevines obtained from vine canopy pixels ($NDVI_{UAV}$) were compared with NDVI values obtained from mixed grapevine and non-grapevine pixels (simulated Satellite NDVI, $NDVI_{SAT}$) in order to assess the impact of image geometrical resolution on LAI and leaf chlorophyll estimation (Fig. 2). In detail, in Experiment 1 $NDVI_{SAT}$ was calculated considering the land area allocated for each vine (3.78 m^2), calculated from the planting distances 0.9 m x 4.2 m) which was then converted in number of pixels by dividing it by the ground sampling distance (GSD, 0.034 m^2) (Fig. 2A). The number of non-grapevine pixels (Fig. 2C) was calculated as the difference between the total number of pixels and the canopy pixels derived by high resolution UAV images (Fig. 2B). The NDVI of bare soil was measured on each flight on 8 one-square-meter soil plots (Fig. 2E) which were periodically tilled to keep it free of weeds. The mean soil NDVI values were then attributed to the non-grapevine pixels. The non-grapevine pixels have been considered as bare soil because in the two study areas the main soil management strategy involves the periodic soil tillage. The NDVI values of bare soil during the entire period of study were quite constant, ranging between 0.08 and 0.1. In Experiment 2 the same procedure was used considering a land area per vine of 2.16 m^2 (planting distances of 0.9 m x 2.4 m).

Two main simplifications with respect to the real field conditions (real $NDVI_{SAT}$) were adopted to simulate the $NDVI_{SAT}$: i) the attribution of NDVI values of bare soil to all non-canopy pixels; ii) the shadows of the canopy, and the corresponding NDVI values, were not taken into account. Since the study was focused in highlighting the effect of different geometrical image resolutions on NDVI values, the above simplifications did not affect the results.

A comparison carried out in 2020 in the Experiment 2 between the real satellite NDVI derived by Sentinel 2 images (Sentinel $NDVI_{SAT}$) at DOY 234 and simulated $NDVI_{SAT}$ derived by UAV images acquired at DOY 239 showed a significant relationship between the two indices (simulated $NDVI_{SAT}$ = 1.19 Sentinel $NDVI_{SAT}$ + 0.03; R^2=0.88).

2.7. Experimental design and statistical analysis

The experiments were carried out on 9 (Experiment 1) and 18 (Experiment 2) grapevines. In each experiment vines were subjected to three different irrigation regimes (3 and 6 vines per irrigation treatment in Experiment 1 and Experiment 2, respectively). The datasets obtained from the multispectral camera (projected canopy area, canopy volume and NDVI) were plotted against ground measurement values (LAI and Chl) and analysed by linear regression using Costat (CoHort Software, Monterey, CA, USA). A multiregression analysis was performed using JMP Pro 17 (SAS Institute Inc., Drive Cary, NC, USA) to assess the contribution of LAI and leaf Chl concentration on $NDVI_{UAV}$ and $NDVI_{SAT}$ values. The Variance Inflation Factors test was performed using JMP Pro 17 (SAS Institute Inc., Drive Cary, NC, USA) to identify the level of multicollinearity between variables.

3. Results

The comparison between the LAI values estimated using the ceptometer and those measured by destructive measurements showed a good correlation (R^2=0.95) (Figure S1). There was a slight overestimation and underestimation of the measured LAI when the number of leaf layers were less and more than 1, respectively (Figure S1). The overestimation was due to the exposure of plant structures other than leaves (shoots, branches and clusters) which intercepted light and therefore were detected by the ceptometer. On the contrary, in denser canopies the contribution of the internal leaf layers to the LAI was underestimated by the ceptometer (Netzer et al., 2009).

The seasonal pattern of leaf Chl content was affected by both growing conditions (potted vs field grown vines) and the irrigation regime (Fig. 3). In Experiment 1, under full irrigation condition leaf Chl

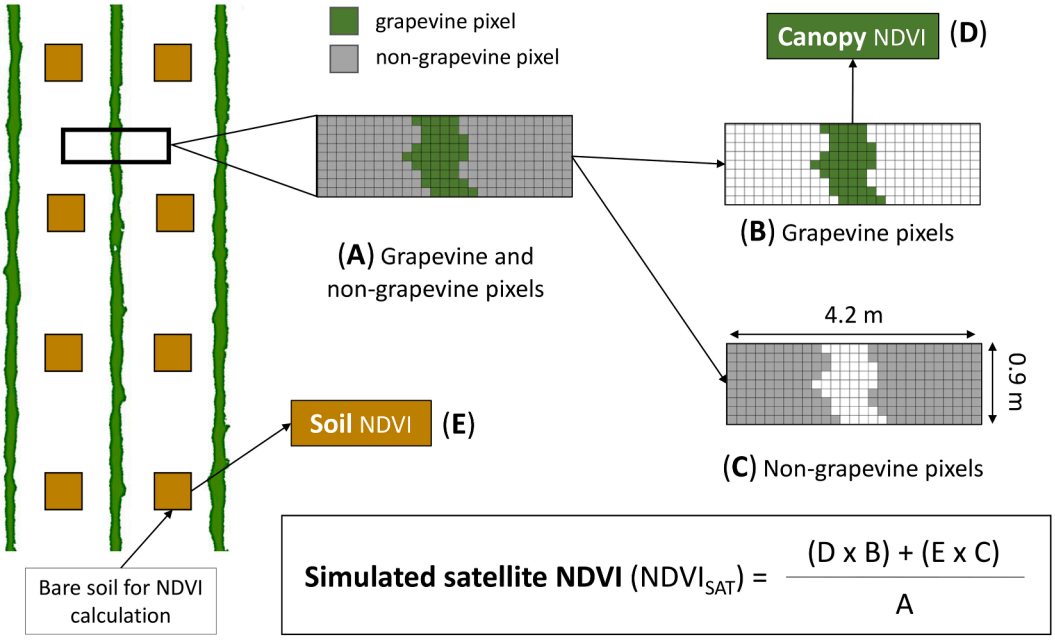

Fig. 2. Schematic representation of the procedure used to calculate the simulated satellite NDVI in Experiment 1. On the left, three vine rows (green) and the eight one-square meter plots (brown) where the NDVI of bare soil was measured at each date of flight. The distance between rows and vines were 4.2 m and 0.9 m, respectively. The same procedure was used in Experiment 2 (planting distance 0.9 × 2.4 m).

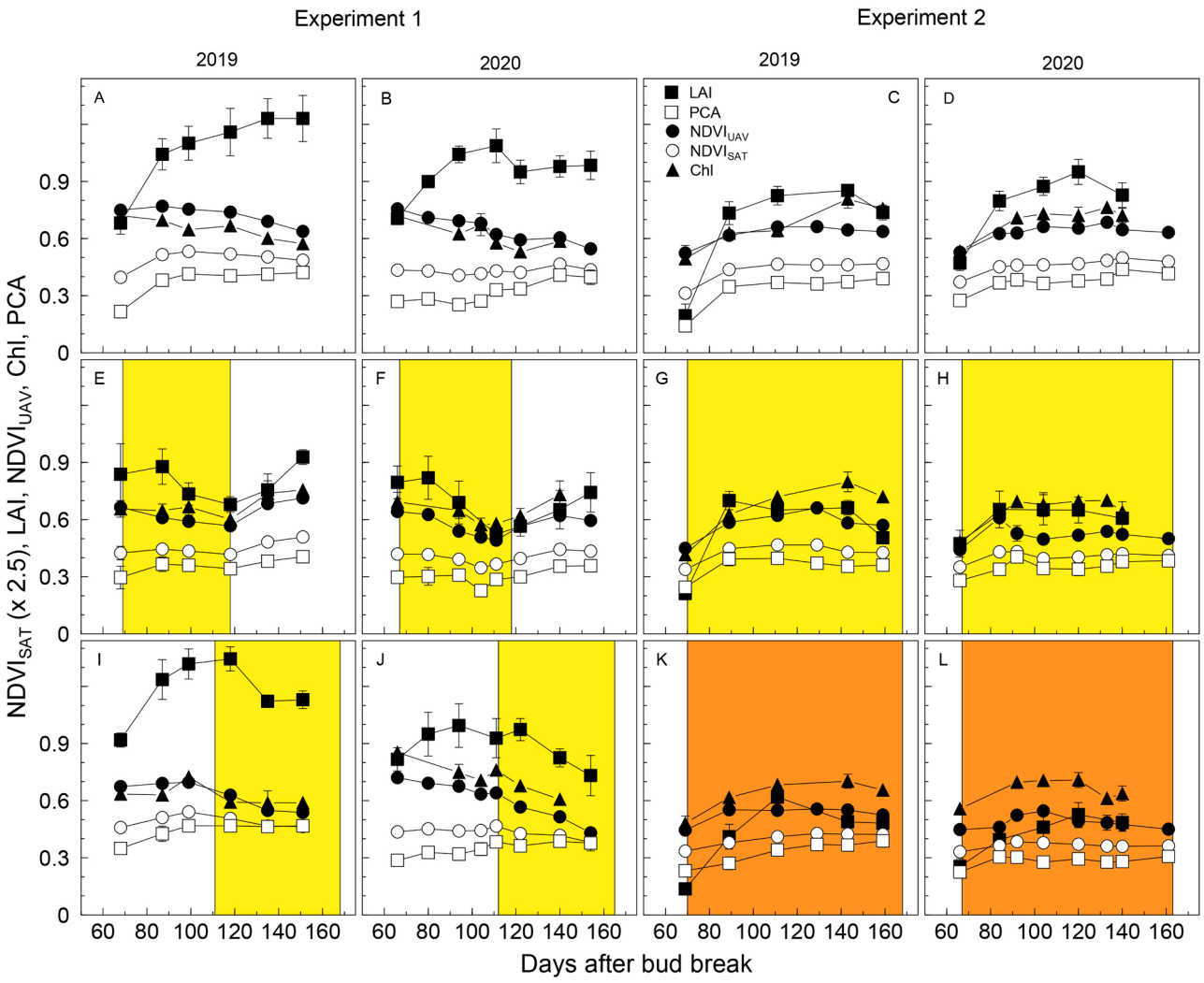

Fig. 3. Seasonal patterns of $NDVI_{UAV}$, $NDVI_{SAT}$, LAI ($m^2\ m^{-2}$), leaf chlorophyll concentration (Chl, g dm^{-2}) and projected canopy area (PCA, m^2) of fully productive Sangiovese grapevines subjected to different growing conditions and irrigation regimes (potted and field-grown vines in Experiment 1 and Experiment 2, respectively) in 2019 (A, E, I, C, G, K) and 2020 (B, F, J, D, H, L). $NDVI_{sat}$ values were multiplied by 2.5 in order to separate the corresponding patterns more clearly in the figure. Experiment 1: FI, potted vines subjected to full irrigation over the entire irrigation period (A, B); RDI-BV, deficit irrigation from fruit set until veraison and full irrigation from veraison until harvest (E, F); RDI-AV, full irrigation from fruit set until veraison and deficit irrigation from veraison until harvest (I, J). Experiment 2: FI, field-grown vines subjected to full irrigation (C, D); DI, deficit irrigation over the entire irrigation period (G, H); RF, rainfed conditions (K, L). Symbols are means ± standard deviations of three (Experiment 1) or six (Experiment 2) vines. The yellow and orange areas indicate the periods when deficit irrigation and rainfed conditions were imposed, respectively.

showed a steady decline after the first date of flight (63 DABB, Fig. 3A, B). This trend was even more dramatic in RDI-AV grapevines, when the water deficit applied after veraison induced a faster reduction in leaf Chl than that observed in FI grapevines (Fig. 3I, J). A different leaf Chl seasonal pattern was observed in RDI-BV grapevines (Fig. 3E, F). The severe water stress applied at fruit set induced a drastic reduction in leaf Chl, which led to minimum values before veraison until the restoration of full irrigation, which caused an increase in leaf Chl (Fig. 3E, F). An opposite trend of leaf Chl was measured in Experiment 2, regardless of the irrigation regime. In all irrigation treatments leaf Chl increased after fruit set, reached its maximum value at 143 (2019) and 133–140 (2020) DABB then declined before harvest (Fig. 3C, D, G, H, K, L).

In both experiments LAI increased in fully-irrigated vines until veraison, then remained quite stable until the last date of measurement (Fig. 3A, B, C, D). Differences emerged between the others irrigation treatments. In Experiment 1, RDI-AV grapevines showed LAI patterns similar to those of FI vines until veraison, when the water restriction induced a reduction in canopy leaf area, due to leaf shedding (Fig. 3I, J). On the contrary, the LAI of RDI-BV vines, decreased before veraison but recovered after veraison when optimal soil water availability was re-established (Fig. 3E, F). In Experiment 2, the moderate and severe water stress induced in SDI and RF treatments, respectively, reduced the leaf area development along the season resulting in lower LAI values than those measured in FI vines (80 and 59% in SDI and RF vines, respectively).

The PCA patterns were quite similar to those of LAI regardless of the irrigation regime in both potted and field-grown vines (Fig. 3). Rapid canopy growth in FI and RDI-AV vines occurred before veraison, while in RDI-BV vines it was limited by the lower soil water availability. The effect of water stress and water replenishment before and after veraison, respectively, was evident on the vegetative growth rate of RDI-BV. After veraison, a slight increase in canopy growth was observed in RDI-BV due to the restoration of full irrigation.

When a decoupling between LAI and leaf Chl was observed (Experiment 1, FI and RDI-AV) $NDVI_{UAV}$ and $NDVI_{SAT}$ showed different trends: $NDVI_{UAV}$ patterns strictly followed the leaf Chl ones, whereas $NDVI_{SAT}$ was more affected by LAI. This, in turn, also resulted in different, and often contrasting, NDVI and LAI patterns in FI and RDI-BV vines. On the

other hand, the water stress and the following recovery experienced by RDI-BV vines resulted in similar trends of $NDVI_{UAV}$ and $NDVI_{SAT}$ (Fig. 3E, F).

Fig. 4 shows the general relationship between $NDVI_{UAV}$ and leaf Chl (R^2=0.30) and between $NDVI_{SAT}$ and leaf Chl (R^2=0.20), including vines of both experiments and all irrigation treatments. The coefficient of determination between $NDVI_{UAV}$ and leaf Chl increased within each site-irrigation regime combination (R^2 of 0.78, 0.74, 0.51, 0.75, 0.60 and 0.54 in Experiment 1, FI, RDI-BV and RDI-AV vines and Experiment 2, FI, SDI and RF vine, respectively). Similar results were measured for $NDVI_{SAT}$ apart from Experiment 1-FI and Experiment 1-RDI-AV combinations (R^2 of 0.01, 0.71, 0.06, 0.76, 0.64 and 0.50 in Experiment 1, FI, RDI-BV and RDI-AV vines and Experiment 2, FI, SDI and RF vine, respectively).

Fig. 5 reports the relationships between the NDVI estimated remotely and the LAI. $NDVI_{SAT}$ was a better predictor of LAI (R^2=0.69) than $NDVI_{UAV}$ (R^2=0.42). Within each site-irrigation regime combination, the best relationships between $NDVI_{UAV}$ and LAI and between $NDVI_{SAT}$ and LAI were measured in Experiment 1-RDI-BV and Experiment 2-FI, respectively (Fig. 5). Differences also emerged between the two experiments. In Experiment 2 the relationships between NDVI (both UAV and SAT) and LAI was tighter than in Experiment 1. In particular, the differences were particularly wide in the FI vines for $NDVI_{UAV}$ (R^2 of 0.06 and 0.89 in Experiment 1 and Experiment 2, respectively) and $NDVI_{SAT}$ (R^2 of 0.46 and 0.90 in Experiment 1 and Experiment 2, respectively).

The multiple regression analysis was used to highlight the impact of LAI and leaf Chl on $NDVI_{UAV}$ and $NDVI_{SAT}$ within each site-irrigation regime combination (Table 1). The results of the variance inflation factors test indicated a low level of multicollinearity between LAI and leaf chlorophyll with values comprised between 1.04 (RDI-BV Experiment 1) and 1.45 (FI Experiment 2). The regression results showed that in potted grapevines (Experiment 1), under full irrigation and RDI-AV regimes, the only variable predictive of $NDVI_{UAV}$ was leaf Chl. Under the same growing conditions, LAI became a significant explanatory variable only in RDI-BV vines (Table 1). In field-grown vines (Experiment 2), regardless of irrigation regime, the LAI was the main predictive variable of $NDVI_{UAV}$ (Table 1). The $NDVI_{UAV}$ of rainfed vines was also significantly affected by leaf chlorophyll values (Table 1). The $NDVI_{SAT}$ was always significantly affected by LAI, regardless of experimental site and irrigation regime (Table 1).

The relationships of LAI with PCA (R^2=0.44) and canopy volume (R^2=0.77) were both significant (Fig. 6). In particular, in both experimental conditions, the canopy volume was a more stable LAI predictor than NDVI, showing minimum (RDI-BV) and maximum (SDI) R^2 values of 0.17 and 0.83, respectively. Canopy volume also showed the best temporal stability in LAI estimation compared to $NDVI_{UAV}$, $NDVI_{SAT}$ and projected canopy area (Supplemental Table 2).

4. Discussion

The results obtained under a wide range of growing conditions allowed us to derive some new and valuable evidence about: i) the specific contribution of LAI and leaf chlorophyll to grapevine canopy $NDVI_{UAV}$; ii) the ability of NDVI from mixed grapevine and non-grapevine pixels (simulated satellite NDVI, $NDVI_{SAT}$) and of the geometrical indices (projected canopy area and canopy volume) derived from multispectral UAV images in estimating grapevine canopy LAI.

In field-grown grapevines (Experiment 2) the LAI and leaf chlorophyll patterns were consistent between each other. The LAI rapidly increased at the beginning of the growing season, remained quite stable around veraison and then began to decrease at a rate depending on soil water availability, in agreement with what reported in previous studies (Picón-Toro et al., 2012; Munitz et al., 2016; Prats-Llinàs et al., 2019; Leolini et al., 2023). Leaf Chl concentration patterns were also consistent to those observed in other experiments on grapevine (Caruso et al., 2017; Casanova-Gascón et al., 2018), showing a rapid increase from leaves unfolding until veraison and then remaining quite stable until the end of the growing season. The accordance between LAI and leaf Chl patterns in field-grown vines resulted, in turn, to similarly shaped NDVI seasonal courses (Fiorillo et al., 2012; Caruso et al., 2017). Under these conditions, it is not possible to discern the specific contribution of LAI and Chl to the canopy NDVI.

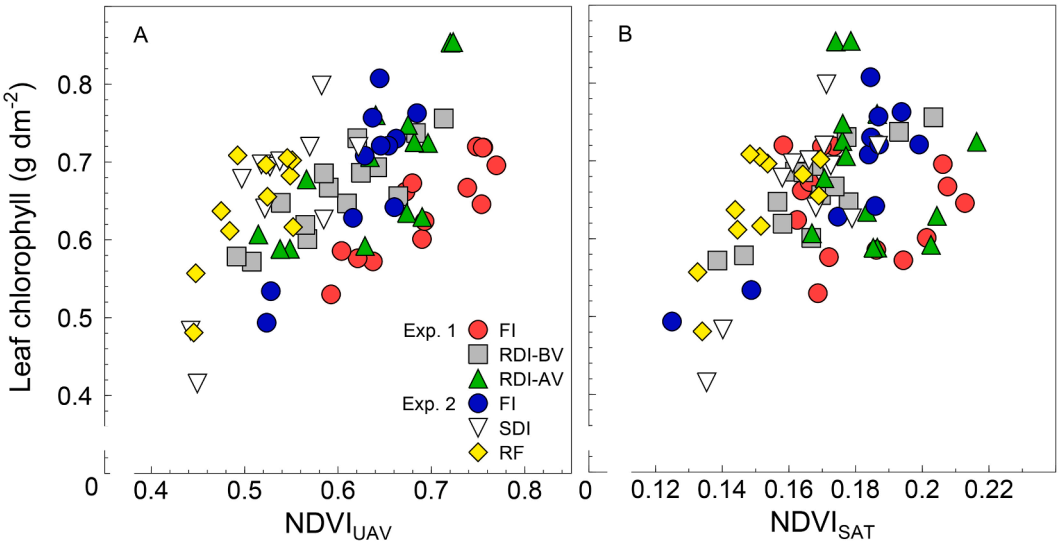

Fig. 4. The relationship between $NDVI_{UAV}$ and leaf chlorophyll concentration (A) and between $NDVI_{UAV}$ and leaf chlorophyll concentration (B) in fully productive "Sangiovese" grapevines subjected to different growing conditions and irrigation regimes (potted and field-grown vines in Experiment 1 and Experiment 2, respectively) in 2019 and 2020. Symbols are means of three (Experiment 1) or six (Experiment 2) vines for each irrigation treatment and date of measurement. Details about irrigation regimes are reported in the caption of Fig. 3 Regression equations are reported only when statistically significant. Equations: General equation (A), Leaf Chl_{ab} = 0.53 $NDVI_{UAV}$ + 0.34, R^2= 0.30; FI (Exp. 1), Leaf Chl_{ab} = 0.88 $NDVI_{UAV}$ + 0.03, R^2= 0.78; RDI-BV, Leaf Chl_{ab} = 0.77 $NDVI_{UAV}$ + 0.20, R^2= 0.74; RDI-AV, Leaf Chl_{ab} = 0.94 $NDVI_{UAV}$ + 0.09, R^2= 0.51; FI (Exp. 2), Leaf Chl_{ab} = 1.60 $NDVI_{UAV}$ -– 0.32, R^2= 0.75; SDI, Leaf Chl_{ab} = 1.53 $NDVI_{UAV}$ -– 0.16, R^2= 0.60; RF, Leaf Chl_{ab} = 1.28 $NDVI_{UAV}$ -– 0.01, R^2= 0.54; General equation (B), Leaf Chl_{ab} = 1.82 $NDVI_{SAT}$ + 0.35, R^2= 0.20; RDI-BV, Leaf Chl_{ab} = 2.85 $NDVI_{SAT}$ + 0.18, R^2= 0.71; FI (Exp. 2), Leaf Chl_{ab} = 3.94 $NDVI_{SAT}$ -– 0.02, R^2= 0.76; SDI, Leaf Chl_{ab} = 5.75 $NDVI_{SAT}$ -– 0.29, R^2= 0.64; RF, Leaf Chl_{ab} = 4.06 $NDVI_{SAT}$ -– 0.03, R^2= 0.50.

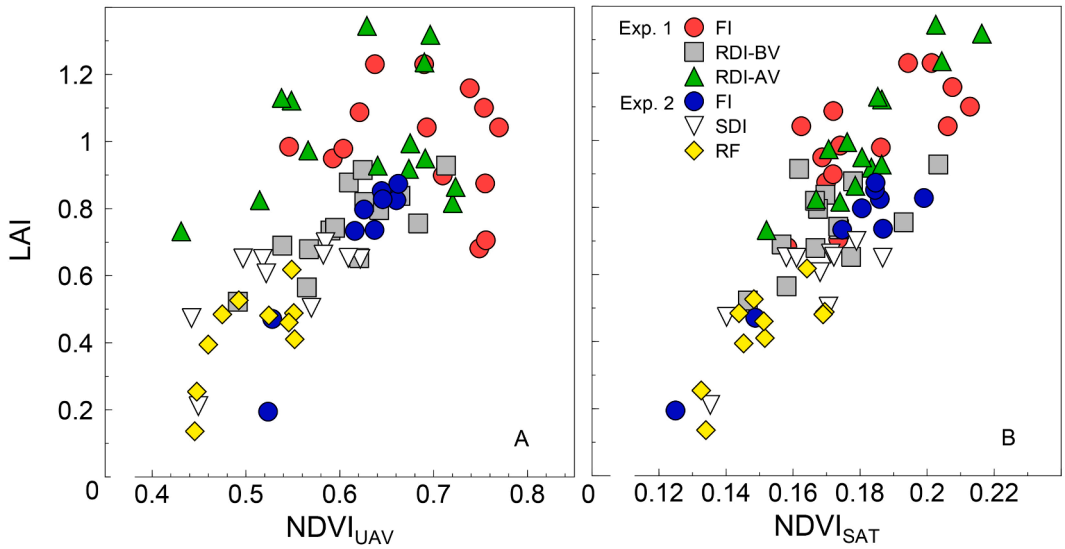

Fig. 5. The relationship between $NDVI_{UAV}$ (NDVI from only vine canopy pixels) and the leaf area index (LAI) (A) and between $NDVI_{SAT}$ (NDVI from mixed grapevine and non-grapevine pixels) and LAI (B) in fully productive "Sangiovese" grapevines subjected to different growing conditions and irrigation regimes (potted and field-grown vines in Experiment 1 and Experiment 2, respectively) in 2019 and 2020. Symbols are means of three (Experiment 1) or six (Experiment 2) vines for each irrigation treatment and date of measurement. Details about irrigation regimes are reported in the caption of Fig. 3. Regression equations are reported only when statistically significant. Equations: General equation (A), LAI = 1.97 $NDVI_{UAV}$ −0.41, R^2 = 0.42; RDI-BV, LAI = 1.60 $NDVI_{UAV}$ - 0.22, R^2= 0.58; FI (Exp. 2), LAI = 4.13 $NDVI_{UAV}$ – 1.83, R^2= 0.89; SDI, LAI = 1.53 $NDVI_{UAV}$ - 0.25, R^2= 0.44; RF, LAI = 2.12 $NDVI_{UAV}$ - 0.64, R^2= 0.47; General equation (B), LAI = 11.18 $NDVI_{SAT}$ – 1.15, R^2= 0.61; RDI-BV, LAI = 4.79 $NDVI_{SAT}$ + 0.07, R^2= 0.32; RDI-AV, LAI = 10.5 $NDVI_{SAT}$ - 0.91, R^2= 0.81; FI (Exp. 2), LAI = 9.72 $NDVI_{SAT}$ - 0.98, R^2= 0.90; SDI, LAI = 7.10 $NDVI_{SAT}$ - 0.59, R^2= 0.61; RF, LAI = 7.88 $NDVI_{SAT}$ - 0.76, R^2= 0.56.

Table 1
Multiregression analysis between $NDVI_{UAV}$, $NDVI_{SAT}$, LAI and Chl indicating the contribution of LAI and Chl on $NDVI_{UAV}$ and $NDVI_{SAT}$ in fully productive "Sangiovese" vines subjected to different growing conditions and irrigation regimes (potted and field-grown vines in Experiment 1 and Experiment 2, respectively) in 2019 and 2020.

Experiment	Irrigation treatments	Predictive variables	p-value (*t*-test)		Std Beta		R^2_{adj}		F (df)		p-value (regression)		RMSE	
			NDVI UAV	NDVI SAT	NDVI UAV	NDVI SAT	NDVI UAV	NDVI SAT	NDVI UAV	NDVI SAT	NDVI UAV	NDVI SAT	NDVI UAV	NDVI SAT
1	FI	Intercept	0.0111	0.0005										
		LAI	0.5570	0.0001	0.071	0.649	0.57	0.34	23.34 (39)	9.60 (39)	0.0001	0.0005	0.046	0.014
		Chl	<0.0001	0.1394	0.791	0.225								
	RDI BV	Intercept	<0.0001	<0.0001										
		LAI	0.0002	<0.0001	0.559	0.631	0.36	0.38	11.37 (39)	12.56 (39)	0.0001	<0.0001	0.050	0.013
		Chl	0.1685	0.7212	0.187	0.047								
	RDI AV	Intercept	0.0347	<0.0001										
		LAI	0.2213	<0.0001	0.177	0.782	0.39	0.54	12.13 (39)	21.15 (39)	0.0001	<0.0001	0.060	0.010
		Chl	<0.0001	0.4003	0.695	0.106								
2	FI	Intercept	<0.0001	<0.0001										
		LAI	0.0009	<0.0001	0.467	0.51	0.43	0.56	19.22 (49)	31.88 (49)	<0.0001	<0.0001	0.047	0.014
		Chl	0.0531	0.0042	0.292	0.347								
	SDI	Intercept	<0.0001	<0.0001										
		LAI	0.0001	<0.0001	0.516	0.696	0.34	0.47	13.49 (49)	22.34 (49)	<0.0001	<0.0001	0.063	0.016
		Chl	0.1219	0.8669	0.194	0.019								
	RF	Intercept	<0.0001	<0.0001										
		LAI	0.0275	0.0012	0.315	0.483	0.30	0.28	11.31 (49)	10.52 (49)	0.0001	0.0002	0.058	0.016
		Chl	0.0414	0.3482	0.350	0.132								

On the contrary, the artificial decoupling of LAI and Chl patterns induced in potted grapevines allowed to evaluate the single out LAI-NDVI and Chl-NDVI relationships, avoiding potential biases due to autocorrelation between LAI and Chl. The divergence between LAI and leaf Chl patterns were evident for FI (during the entire irrigation period) and RDI-AV potted vines (only before veraison). LAI showed a pattern similar to that of field-grown vines, whereas leaf chlorophyll concentration in potted vines declined earlier in the season. Previous studies reported divergences between grapevine nitrogen content and canopy biomass as a consequence of different canopy management techniques (Weyland et al., 2006; Spring et al., 2012). The constant decline from fruit set shown by the $NDVI_{UAV}$ under these conditions suggests a higher contribution of leaf chlorophyll than LAI to canopy NDVI from vine canopy pixels. The water stress applied to the RDI-BV

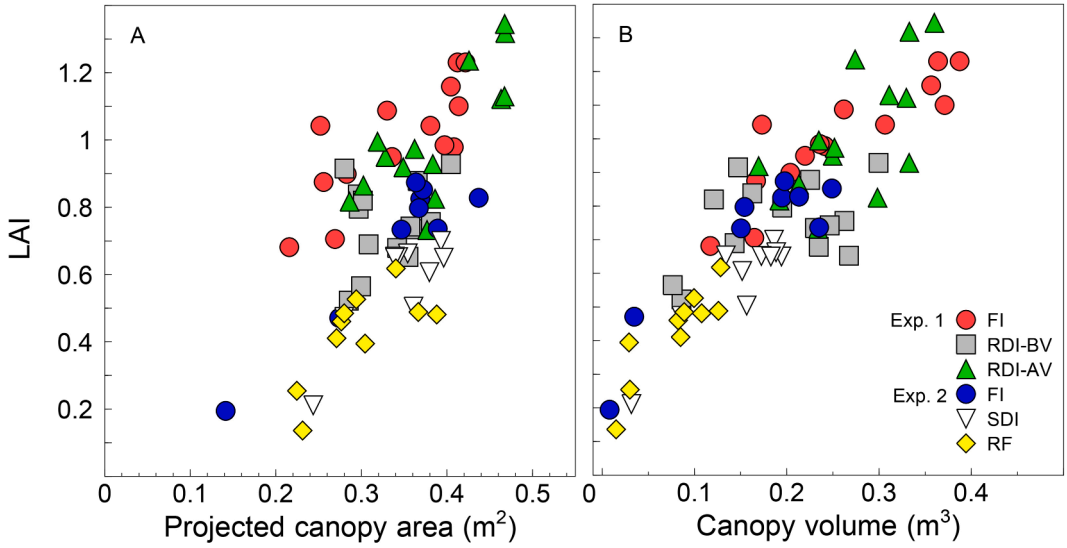

Fig. 6. The relationship between projected canopy area (PCA) and the leaf area index (LAI) (A) and between canopy volume (CV) and LAI (B) in fully productive "Sangiovese" vines subjected to different growing conditions and irrigation regimes (potted and field-grown vines in Experiment 1 and Experiment 2, respectively) in 2019 and 2020. Symbols are means of three (Experiment 1) or six (Experiment 2) vines for each irrigation treatment and date of measurement. Details about irrigation regimes are reported in the caption of Fig. 3. Regression equations are reported only when statistically significant. Equations: General equation (A), LAI = 2.72 PCA – 0.16, R^2 = 0.44; FI (Exp. 1), LAI = 1.79 PCA + 0.38, R^2 = 0.61; RDI-AV, LAI = 2.26 PCA + 0.14, R^2 = 0.59; FI (Exp. 2), LAI = 2.56 PCA – 0.15, R^2 = 0.85; SDI, LAI = 2.53 PCA – 0.29, R^2 = 0.69; RF, LAI = 1.82 PCA – 0.11, R^2 = 0.50; General equation (B), LAI = 2.50 CV + 0.29, R^2 = 0.77; FI (Exp. 1), LAI = 1.69 CV + 0.57, R^2 = 0.78; RDI-BV, LAI = 0.72 CV + 0.61, R^2 = 0.17; RDI-AV, LAI = 2.16 CV + 0.43, R^2 = 0.44; FI (Exp. 2), LAI = 2.49 CV + 0.31, R^2 = 0.82; SDI, LAI = 2.56 CV + 0.19, R^2 = 0.83; RF, LAI = 2.79 CV + 0.21, R^2 = 0.82.

vines resulted in better consistency between LAI and leaf Chl and, in turn, with NDVI $_{UAV}$. The specific relationships between $NDVI_{UAV}$ and leaf chlorophyll concentration and between $NDVI_{UAV}$ and LAI under the different growing conditions and irrigation regimes confirmed this finding. $NDVI_{UAV}$ was significantly correlated with leaf Chl, regardless of experimental sites and irrigation regimes (R^2 comprised between 0.51 and 0.78). On the contrary, $NDVI_{UAV}$ was unable to predict LAI in potted vines subjected to full irrigation and water stress after veraison (Fig. 5A). The multiple regression analysis further confirmed our hypothesis that under specific growing conditions (high canopy biomass and low leaf chlorophyll concentration) $NDVI_{UAV}$ was more affected by leaf chlorophyll concentration than LAI, whereas the latter was always a significant explanatory variable of $NDVI_{SAT}$. The divergences between NDVI-LAI-Chl patterns are usually not evident under field conditions and, to the best of our knowledge, this is the first study documenting this aspect.

The seasonal patterns of $NDVI_{SAT}$ were quite similar to those of LAI. Unlike $NDVI_{UAV}$, $NDVI_{SAT}$ was well correlated with LAI, regardless of growing conditions and irrigation (R^2 comprised between 0.32 and 0.90). It turns out that $NDVI_{UAV}$ has a tight correlation with leaf Chl whereas LAI has a greater impact on $NDVI_{SAT}$. These results may be explained considering the different information included in $NDVI_{UAV}$ and $NDVI_{SAT}$ values. Canopy $NDVI_{UAV}$, obtained from high-resolution UAV images, represents the mean NDVI value of the only vine canopy pixels and, thus, it is more affected by the plant physiological activity (e.g. leaf chlorophyll and photosynthetic rate) than by its biomass (e.g. projected canopy area and LAI). On the contrary, $NDVI_{SAT}$ integrates reflectance information of both canopy and soil and, therefore, it is more affected by the variation in the fractional vegetation cover than by the vine physiology (Gitelson et al., 2002). Similar results have been reported in previous studies where NDVI was derived from satellite multispectral images (Carlson et al., 1997; Hall et al., 2002; Johnson et al., 2003). Johnson et al. (2003) compared the seasonal patterns (3 June – September 4) of field measured LAI and NDVI derived from Ikonos multispectral satellite images in five vineyard blocks characterized by different planting distances, cultivars, training system and age. The temporal progression of NDVI and LAI showed a general consistency between the two parameters and a good correlation (R^2=0.92) between each other was also found when all dates of measurements were pooled together. Hall et al. (2008) analysed the relative contribution of grapevine projected canopy area derived from high-resolution aerial images to the leaf area index, concluding that the correlations between NDVI and LAI reported in previous studies based on low-resolution imagery most likely relied on the proxy relationship between NDVI and canopy area. In this study, this assumption was confirmed by simulating the canopy satellite NDVI ($NDVI_{SAT}$) and comparing it with $NDVI_{UAV}$, PCA and LAI.

The regression analyses showed that canopy volume derived by UAV was a better predictor of LAI than $NDVI_{UAV}$ and $NDVI_{SAT}$. Previous studies carried out on orchards and vineyards assessed the reliability of geometrical canopy data (3D point cloud, canopy volume, projected canopy area, canopy height) derived by UAV imagery for LAI estimation (Mathews and Jensen 2013; Ballesteros et al., 2015; Comba et al., 2020; Caruso et al., 2022c; Padua et al., 2022). In this study, the correlation between canopy volume and LAI was almost always significant, regardless of growing conditions, irrigation treatment and phenological stage, highlighting a better temporal stability over the growing season compared with the $NDVI_{UAV}$-LAI and $NDVI_{SAT}$-LAI relationships. The strength of the relationship can be attributable to the geometrical nature of the two compared indices (canopy volume and LAI), allowing to exclude the physiological and biochemical parameters (leaf age, leaf chlorophyll content, leaf photosynthesis) of the canopy which, as mentioned above, may be responsible for bias in the LAI estimation.

5. Conclusions

Irrigation significantly affected biophysical parameters and canopy NDVI in both potted and field-grown vines. The comparison of NDVI, LAI and leaf chlorophyll of grapevine under different growing conditions and irrigation regimes allows to confirm the two main hypotheses behind this experiment. First, the leaf chlorophyll concentration has a greater impact than LAI on NDVI values obtained from vine canopy pixels ($NDVI_{UAV}$), whereas $NDVI_{SAT}$ is more affected by LAI. This is due to the different main information included in $NDVI_{UAV}$ (leaf pigments)

and $NDVI_{SAT}$ (geometrical canopy characteristics). These results also highlight the questionable informative value of NDVI in distinguish specific abiotic (water and nutrient) stresses in the vineyard.

Secondly, the canopy volume from UAV images is a better predictor of LAI ($R^2 = 0.77$) than NDVI (R^2 of 0.42 and 0.61 for $NDVI_{UAV}$ and $NDVI_{SAT}$, respectively) and the resulting relationship presents a better temporal stability. From a practical point of view, this implies that the UAV geometric indices can be effectively used to monitor the biomass of the canopy during the entire growing season and under conditions of environmental stress.

CRediT authorship contribution statement

Giovanni Caruso: Conceptualization, Data curation, Formal analysis, Funding acquisition, Investigation, Methodology, Resources, Software, Supervision, Validation, Writing – original draft. **Giacomo Palai:** Data curation, Formal analysis, Investigation, Software, Validation, Visualization, Writing – review & editing. **Letizia Tozzini:** Investigation, Writing – review & editing. **Claudio D'Onofrio:** Funding acquisition, Resources, Writing – review & editing. **Riccardo Gucci:** Funding acquisition, Resources, Writing – review & editing.

Declaration of Competing Interest

The authors declare that they have no known competing financial interests or personal relationships that could have appeared to influence the work reported in this paper.

Data availability

Data will be made available on request.

Acknowledgments

This research was supported by NETAFIM Italy, project "Identification of optimal irrigation strategies for grapevine, olive and hazelnut". We are grateful to M. Frassi and M. Di Giacomo for their technical assistance.

Supplementary materials

Supplementary material associated with this article can be found, in the online version, at doi:10.1016/j.scienta.2023.112398.

References

Ballesteros, R., Ortega, J.F., Hernández, D., Moreno, M.A., 2015. Characterization of *Vitis vinifera* L. canopy using unmanned aerial vehicle-based remote sensing and photogrammetry techniques. Am. J. Enol. Vitic. 66, 120–129.

Bonilla, I., de Toda, F.M., Martìnez-Casanovas, J.A., 2015. Vine vigor, yield and grape quality assessment by airborne remote sensing over three years: analysis of unexpected relationships in cv. Tempranillo. Span. J. Agric. Res. 13, 1–8.

Bramley, R.G.V., 2001. Variation in yield and quality of winegrapes and the effect of soil property variation in two contrasting Australian vineyards. In: Proc. 3rd Europ. Conf. Prec. Agric, 2, pp. 767–772.

Campos, J., García-Ruíz, F., Gil, E., 2021. Assessment of vineyard canopy characteristics from vigour maps obtained using UAV and satellite imagery. Sensors 21 (7), 2363.

Carlson, T.N., Ripley, D.A., 1997. On the relation between NDVI, fractional vegetation cover, and leaf area index. Remote Sens. Environ. 62 (3), 241–252.

Caruso, G., Tozzini, L., Rallo, G., Primicerio, J., Moriondo, M., Palai, G., Gucci, R., 2017. Estimating biophysical and geometrical parameters of grapevine canopies ('Sangiovese') by an unmanned aerial vehicle (UAV) and VIS-NIR cameras. Vitis 56, 63–70.

Caruso, G., Zarco-Tejada, P.J., Gonzalez-Dugo, V., Moriondo, M., Tozzini, L., Palai, G., Rallo, G., Hornero, A., Primicerio, J., Gucci, R., 2019. High-resolution imagery acquired from an unmanned platform to estimate biophysical and geometrical parameters of olive trees under different irrigation regimes. PLoS ONE 14, 0210804.

Caruso, G., Palai, G., Marra, F.P., Caruso, T., 2021. High-resolution UAV imagery for field olive (*Olea europaea* L.) phenotyping. Horticulturae 7, 258.

Caruso, G., Palai, G., Gucci, R., Priori, S., 2022a. Remote and proximal sensing techniques for site-specific irrigation management in the olive orchard. Appl. Sci. 12, 1309.

Caruso, G., Palai, G., Gucci, R., D'Onofrio, C., 2022b. The effect of regulated deficit irrigation on growth, yield, and berry quality of grapevines (cv. Sangiovese) grafted on rootstocks with different resistance to water deficit. Irr. Sci. 41, 453–467.

Caruso, G., Palai, G., Tozzini, L., Gucci, R., 2022c. Using visible and thermal images by an unmanned aerial vehicle to monitor the plant water status, canopy growth and yield of olive trees (cvs. Frantoio and Leccino) under different irrigation regimes. Agronomy 12, 1904.

Casanova-Gascón, J., Martín-Ramos, P., Martí-Dalmau, C., Badía-Villas, D., 2018. Nutrients assimilation and chlorophyll contents for different grapevine varieties in calcareous soils in the Somontano DO (Spain). Beverages 4, 90.

Comba, L., Biglia, A., Ricauda Aimonino, D., Tortia, C., Mania, E., Guidoni, S., Gay, P., 2020. Leaf Area Index evaluation in vineyards using 3D point clouds from UAV imagery. Prec. Agric. 21, 881–896.

Coombe, B.G., 1995. Growth stages of the grapevine: adoption of a system for identifying grapevine growth stages. Aust. J. Grape Wine Res. 1, 104–110.

Di Gennaro, S.F., Dainelli, R., Palliotti, A., Toscano, P., Matese, A., 2019. Sentinel-2 validation for spatial variability assessment in overhead trellis system viticulture versus UAV and agronomic data. Remote Sens 11 (21), 2573.

Dobrowski, S.Z., Ustin, S.L., Wolpert, J.A., 2003. Grapevine dormant pruning weight prediction using remotely sensed data. Aust. J. Grape Wine Res. 9, 177–182.

Elazab, A., Ordóñez, R.A., Savin, R., Slafer, G.A., Araus, J.L., 2016. Detecting interactive effects of N fertilization and heat stress on maize productivity by remote sensing techniques. Eur. J. Agron. 73, 11–24.

Fiorillo, E., Crisci, A., De Filippis, T., Di Gennaro, S.F., Di Blasi, S., Matese, A., Primicerio, J., Vaccari, F.P., Genesio, L., 2012. Airborne high-resolution images for grape classification: changes in correlation between technological and late maturity in a Sangiovese vineyard in Central Italy. Aust. J. Grape Wine Res. 18, 80–90.

Gitelson, A.A., Kaufman, Y.J., Stark, R., Rundquist, D.C., 2002. Novel algorithms for remote estimation of vegetation fraction. Remote Sens. Environ. 80, 76–87.

Gitelson, A.A., 2004. Wide dynamic range vegetation index for remote quantification of biophysical characteristics of vegetation. J. Plant Physiol. 161, 165–173.

Haboudane, D., Miller, J.R., Pattey, E., Zarco-Tejada, P.J., Strachan, I.B., 2004. Hyperspectral vegetation indices and novel algorithms for predicting green LAI of crop canopies: modeling and validation in the context of precision agriculture. Remote Sens. Environ. 90, 337–352.

Hall, A., Lamb, D.W., Holzapfel, B., Louis, J., 2002. Optical remote sensing applications in viticulture-a review. Aust. J. Grape Wine Res 8, 36–47.

Hall, A., Louis, J.P., Lamb, D.W., 2008. Low-resolution remotely sensed images of winegrape vineyards map spatial variability in planimetric canopy area instead of leaf area index. Aust. J. Grape Wine Res. 14, 9–17.

Johnson, L.F., Roczen, D.E., Youkhana, S.K., Nemani, R.R., Bosch, D.F., 2003. Mapping vineyard leaf area with multispectral satellite imagery. Comp. Elec. Agric. 38, 33–44.

Khaliq, A., Comba, L., Biglia, A., Ricauda Aimonino, D., Chiaberge, M., Gay, P., 2019. Comparison of satellite and UAV-based multispectral imagery for vineyard variability assessment. Remote Sens. 11, 436.

Lamb, D.W., Weedon, M.M., Bramley, R.G.V., 2004. Using remote sensing to predict grape phenolics and colour at harvest in a cabernet sauvignon vineyard: timing observations against vine phenology and optimising image resolution. Aust. J. Grape Wine Res. 10, 46–54.

Leolini, L., Bregaglio, S., Ginaldi, F., Costafreda-Aumedes, S., Di Gennaro, S.F., Matese, A., Maselli, F., Caruso, G., Palai, G., Bajocco, S., Bindi, M., Moriondo, M., 2023. Use of remote sensing-derived fPAR data in a grapevine simulation model for estimating vine biomass accumulation and yield variability at sub-field level. Precision Agric 24, 705–726.

Matese, A., Toscano, P., Di Gennaro, S.F., Genesio, L., Vaccari, P., Primicerio, J., Belli, C., Zaldei, A., Bianconi, R., Gioli, B., 2015. Intercomparison of UAV, aircraft and satellite remote sensing platforms for precision viticulture. Remote Sens 7, 2971–2990.

Matese, A., Di Gennaro, S.F., 2021. Beyond the traditional NDVI index as a key factor to mainstream the use of UAV in precision viticulture. Sci. Rep. 11 (1), 1–13.

Mathews, A.J., Jensen, J.L.R., 2013. Visualizing and quantifying vineyard canopy LAI using an Unmanned Aerial Vehicle (UAV) collected high density structure from motion point cloud. Remote Sens 5 (5), 2164–2183.

Munitz, S., Netzer, Y., Schwartz, A., 2016. Sustained and regulated deficit irrigation of field-grown Merlot grapevines. Aust. J. Grape Wine Res. 23 (1), 87–94.

Netzer, Y., Yao, C., Shenker, M., Bravdo, B.A., Schwartz, A., 2009. Water use and the development of seasonal crop coefficients for superior seedless grapevines trained to an open-gable trellis system. Irr. Sci. 27, 109–120.

Pádua, L., Chiroque-Solano, P.M., Marques, P., Sousa, J.J., Peres, E., 2022. Mapping the Leaf Area Index of *Castanea sativa* Miller using UAV-based multispectral and geometrical data. Drones 6, 422.

Palai, G., Caruso, G., Gucci, R., D'Onofrio, C., 2022. Berry flavonoids are differently modulated by timing and intensities of water deficit in *Vitis vinifera* L. cv. Sangiovese. Front. Plant Sci. 13, 1040899.

Picón-Toro, J., González-Dugo, V., Uriarte, D., Mancha, L.A., Testi, L., 2012. Effects of canopy size and water stress over the crop coefficient of a "Tempranillo" vineyard in south-western Spain. Irrig. Sci. 30, 419–432.

Prats-Llinàs, M.T., Bellvert, J., Mata, M., Marsal, J., Girona, J., 2019. Post-harvest harvest regulated deficit irrigation in chardonnay did not reduce yield but at long-term, it could affect berry composition. Agronomy 9, 328.

Rey-Caramés, C., Diago, M.P., Martín, M.P., Lobo, A., Tardaguila, J., 2015. Using RPAS multi-spectral imagery to characterise vigour, leaf development, yield components and berry composition variability within a vineyard. Remote Sens. 7, 14458–14481.

Rouse, J.W., Haas, R.H., Schell, J.A., Deering, D.W., 1974. Monitoring vegetation systems in the Great Plains with ERTS. NASA Spec. Publ 351 (1), 309.
Sims, D.A., Gamon, J.A., 2002. Relationships between leaf pigment content and spectral reflectance across a wide range of species, leaf structures and developmental stages. Remote Sens. Environ. 81, 337–354.
Smart, R., Robinson, M., 1991. Point quadrat. Sunlight into wine: a Handbook for Winegrape Canopy Management. Winetitles, Underdale, SA, Australia.
Spring, J.L., Verdenal, T., Zufferey, V., Viret, O., 2012. Nitrogen dilution in excessive canopies of Chasselas and Pinot noir cvs. J. Inter. Sci. Vigne Vin 46 (3), 233–240.
Sun, L., Gao, F., Anderson, M.C., Kustas, W.P., Alsina, M.M., Sanchez, L., Sams, B., McKee, L., Dulaney, W., White, W.A., Alfieri, J.G., Prueger, J.H., Melton, F., Post, K., 2017. Daily mapping of 30m LAI and NDVI for grape yield prediction in California vineyards. Remote Sens 9, 317.
Tan, C.-W., Zhang, P.-P., Zhou, X.-X., Wang, Z.-X., Xu, Z.-Q., Mao, W., Li, W.-X., Huo, Z.-Y., Guo, W.-S., Yun, F., 2020. Quantitative monitoring of leaf area index in wheat of different plant types by integrating NDVI and Beer-Lambert law. Sci. Rep. 10, 929.
Verdenal, T., Dienes-Nagy, Á., Spangenberg, J.E., Zufferey, V., Spring, J.L., Viret, O., Marin-Carbonne, J., Van Leeuwen, C., 2021. Understanding and managing nitrogen nutrition in grapevine: a review. Oeno One 55 (1), 1–43.
Weyand, K.M., Schultz, H.R., 2006. Long-term dynamics of nitrogen and carbohydrate reserves in woody parts of minimally and severely pruned Riesling vines in a cool climate. Am. J. Enol. Vitic. 57 (2), 172–182.
White, W.A., Alsina, M.M., Nieto, H., McKee, L.G., Gao, F., Kustas, W.P., 2019. Determining a robust indirect measurement of leaf area index in California vineyards for validating remote sensing-based retrievals. Irr. Sci. 37 (3), 269–280.
Zarco-Tejada, P.J., Berjón, A., Lopez-Lozano, R., Miller, J.R., Martín, P., Cachorro, V., González, M.R., De Frutos, A., 2005. Assessing vineyard condition with hyperspectral indices: leaf and canopy reflectance simulation in a row-structured discontinuous canopy. Remote Sens. Environ. 99 (3), 271–287.